PseudoCell: A collaborative network for *in silico* prediction of regulatory pathways

Vinícius Pierdoná[1], Patrícia Lavandoski[1], Rafael Moura Maurmann[2], Guilherme Antônio Borges[3,4], José Carlos Merino Mombach[5], Fátima Theresinha Costa Rodrigues Guma[1] and Florencia María Barbé-Tuana[2,6*]

[1] Programa de Pós-Graduação em Ciências Biológicas: Bioquímica do Departamento de Bioquímica, Universidade Federal do Rio Grande do Sul, Porto Alegre, Rio Grande do Sul, 90035-003, Brasil.
[2] Programa de Pós-Graduação em Biologia Celular e Molecular da Escola de Ciências da Saúde e da Vida - Pontifícia Universidade Católica do Rio Grande do Sul, Porto Alegre, Rio Grande do Sul, 90619-900, Brasil.
[3] Departamento de Engenharia Electrotécnica e de Computadores, Universidade de Coimbra, Coimbra, 3030-290, Portugal
[4] Departamento de Ensino, Pesquisa e Extensão - Instituto Federal Sul-rio-grandense, Campus Charqueadas, Rio Grande do Sul, 96745-000, Brasil
[5] Departamento de Física, Universidade Federal de Santa Maria, Santa Maria, Rio Grande do Sul, Brasil
[6] Programa de Pós-Graduação em Pediatria e Saúde de Criança da Escola de Medicina, Pontifícia Universidade Católica do Rio Grande do Sul, Porto Alegre, Rio Grande do Sul, 90619-900, Brasil.

* To whom correspondence should be addressed: Florencia María Barbé-Tuana, PhD.
Florencia.tuana@pucrs.br
School of Sciences, Health and Life, Pontifical Catholic University of Rio Grande do Sul. Address: Avenida Ipiranga 6681, P12D - 401, Porto Alegre, RS, Brazil, ZIP-Code: 90619-900. Phone number: +55 51 3353-6037.

ABSTRACT

We introduce PseudoCell, an open-source regulatory network and simulation tool implemented in Java for the analysis of biological network dynamics. PseudoCell provides a customizable and scalable regulatory network of 572 cellular and molecular elements. Based on a systemic perspective, the PseudoCell tool implements a set of computational methods for asynchronous logical model simulation, including the definition of perturbations in constant or pulsatile frequency, as well as knockout emulation. The current version also provides a framework for exporting users´ modifications from the network to an online database, as well as importing updated versions. Finally, we validate our results with *ex vivo* experiments and demonstrate that *in silico* data generated with PseudoCell can qualitatively reproduce expected findings in the face of increasing stimuli with eotaxin-1 (CCL11) in human peripheral blood mononuclear cells.

1. Introduction

The study of modern molecular and cellular biology is largely based on a mechanistic and deterministic theoretical framework. This reductionist paradigm presupposes a unidirectional flow of information organized in linear and predictive systems. In this sense, the molecular relationships that occur in a cellular condition are described from a deterministic perspective, within a linear system (Bizzarri et al., 2013; Mazzocchi, 2008).

This approach contributed decisively to the construction of the knowledge on which molecular biology is grounded. However, despite reductionism having proved to be a powerful and productive methodology, the highly integrative character of the molecular components, their intrinsically stochastic dynamics, and cellular heterogeneity impose important limitations within this paradigm (Bhalla & Iyengar, 1999; Elowitz, 2013). Indeed, it has been demonstrated that it is rarely possible for any cellular outcome to be the result of a single molecule (Barabási & Oltvai, 2004). This suggests that biological phenomena result from the interaction between different molecular and cellular components at multiple levels of complexity. These interactions build interdependent biological networks that together orchestrate the molecular landscape of the cell (Jordan et al., 2000; Kitano, 2002a).

The systemic paradigm aims to provide a theoretical framework that can account for the inherent complexity, stochasticity, and non-linearity of biological systems (Coveney & Fowler, 2005; Kitano, 2002a). In this sense, an important challenge toward a proper understanding of biological functions is the creation of methods that allow us to evaluate the dynamics arising from these interactions. Within this perspective, the *in silico* study of biological networks presents itself as a powerful tool to structure and understand the spatial and dynamic organization of these biological systems (Fisher et al., 2014; Fisher & Henzinger, 2007; Helikar et al., 2012; Kitano, 2002b; Naldi et al., 2018; Ostaszewski et al., 2021). Among the existing methodologies and formalisms in this field, the logical modeling of biological networks stands out due to its flexibility and high predictive power (Béal et al., 2021; Gupta et al., 2020a, 2020b, 2022; Gupta & Hashimoto, 2022; Rodríguez-Jorge et al., 2019; Saadatpour & Albert, 2013; Samaga & Klamt, 2013; Silveira et al., 2020).

Briefly, in logical modeling, each modeled element is reduced to a node in the network and is associated with a numerical variable that is, commonly, a boolean. The relationships between these elements are represented as links in the network. These links can denote two types of interactions: direct interactions, such as the physical association in the formation of a molecular complex; or indirect interactions, such as the expression stimulation induced by a transcription factor. These relationships are then described in the form of logical activation or inhibition rules. This structure allows computing the state of a given node in the face of changes in neighboring nodes (Jordan et al., 2000; Saadatpour & Albert, 2013; Samaga & Klamt, 2013).

Several tools have been proposed to address the challenge of logical modeling, including GINsim and BioLQM (Naldi, 2018; Naldi et al., 2018). These tools have made significant contributions to the field, but their utilization demands a comprehensive understanding of logical modeling. To simulate experimental conditions, non-expert users must spend a substantial amount of time familiarizing themselves with the techniques involved in constructing logical models and obtaining literature-based information to implement the desired network. Additionally, although they allow network importation, no tool presently has a broad native network, and the imported networks are often limited in scope. Therefore, a tool that incorporates a wide native network and offers a user-friendly interface for simulating disruptions or knockouts in the network could prove advantageous.

In this paper, we introduce PseudoCell, an open-source regulatory network and simulation tool designed to evaluate the behavior of cellular and molecular networks from a systems biology perspective.

2. Network Definition

The construction of a biological logical network permeates the abstraction of its elements. Cellular or molecular elements such as proteins, genes, metabolites, or even abstract entities, such as cellular outcomes, are reduced to nodes. Thus, to be able to understand the intermolecular relationships that the nodes trace among themselves, it is essential to understand how the biological signal propagates in a network. In this sense, signal propagation can happen through two main mechanisms, through interactions between proteins or the degradation and synthesis of new molecules (Bhalla & Iyengar, 1999). In a biological network, therefore, these two forms of signal propagation can be reduced to links or edges between two nodes. In this way, each link represents the abstraction of the relationship of activation or inhibition between two network elements. Currently, the PseudoCell network consists of 572 nodes divided between 527 genes, proteins, and cellular events, and 45 metabolites connected by 1,179 positive (activation) and negative (inhibition) directional edges (Figure 1).

Furthermore, to compute the activation or inhibition interaction between nodes, variables are assigned to each network element, representing its activation state at a given moment. For that, the state of a node abstracts the expression, phosphorylation, or even concentration of a determined molecule. In PseudoCell the state of a given node *n* was

given by a discrete or continuous number and assumed values in the interval [0, Max_n], where Max_n is the maximum state value described for that component. Whenever possible, boolean values were assumed to describe the activation state of the nodes to represent the threshold from which this element can elucidate a certain biological effect.

In PseudoCell network construction, new pathways were added in two steps: creation and verification. That is, for each new pathway added, it was verified whether the network behaved according to the experimental data found in the literature. This methodology was chosen to increase the reliability of the generated network. However, it is essential to recognize that specific experimental conditions may require specific interpretations of the interactions between nodes. Thus, to meet the user's goals, the PseudoCell interface implements functions for editing nodes or logic rules, as described in another section of this paper.

To guarantee a non-deterministic behavior to the model, the nodes were updated asynchronously and not in parallel. For this purpose, a randomly organized list of elements was generated at each algorithm update cycle. In this way, at each update cycle all nodes are updated in random order.

3. PseudoCell: Software Organization and Functionalities

PseudoCell is a Java-based regulatory network and simulation tool that allows users to evaluate network dynamics in response to disturbances or stimuli of a specific node over time. The tool employs the logical formalism described earlier and allows continuous or pulsatile perturbations. Additionally, PseudoCell facilitates the expansion and modification of its network and supports the importing and exporting of networks implemented by other users.

PseudoCell is organized into three major modules: the core module, the user interface module, and the export/import module (Figure 2). The core module is responsible for handling the logic rules that govern the behavior of the biological network. This module is the backbone of PseudoCell, as it is responsible for processing and implementing the logic rules that drive the simulation. The user interface module is divided into three sub-modules: General Configurations, Node Configurations, and Rules Configurations. The General Configurations sub-module receives and processes the experimental conditions and simulation settings determined by the user. This includes the number of times the network will be updated at each simulation, the number of times the simulation will be

repeated (Sample Size, S), and the network activation stimuli. Here, the user can choose the stimulated node and its stimulus frequency.

In the Node Configurations sub-module, the user can create or edit the information referring to any node in the network. This allows the expansion of the original network and the inclusion of additional nodes to increase the accuracy of the simulation. Additionally, the user can knockdown any node, which simulates the effect of gene knockout or protein depletion on the network behavior.

In the Rules Configurations sub-module, the user can edit or create rules for all network nodes. These rules govern the behavior of each node and define the relationships between nodes in the network. By allowing the user to modify these rules, PseudoCell provides a high degree of flexibility and customization.

Finally, the import/export module guarantees data persistence and allows the user to share their networks with the community or absorb network updates made by the community in their own experiments. This module allows for the seamless exchange of data between PseudoCell users, enabling collaboration and sharing of knowledge.

3.1. Simulation and Output

The main function of the tool is to perform analysis of network dynamics in response to different stimuli. In this sense, the stimuli provided to the network aim to emulate those applied to biological systems, such as the activation of a particular receptor or the increase/decrease in the expression of a given protein. Also, these analyses can be performed either to understand the behavior of a specific element within the context simulated in the network or to understand the dynamic responses of the network itself through the evaluation of the general behavior of the nodes.

After the execution of each sample, the tool computes the activation frequency of all nodes in the network. For each node, the activation frequency (F_n) is calculated through the equation below (Equation 1) where St_n represents the status of that node and t represents the total number of update cycles. For Boolean nodes, the activation frequency also represents the probability of that element being activated at any given moment. Thus, the result is an array in which each position is occupied by the activation frequency of a node.

$$F_n = \frac{\sum \quad St_n}{t} \tag{1}$$

Upon completion of the experiment, the tool generates a matrix where each row corresponds to the result array of each sample (S1, S2…Sn). This array is then exported as a Comma Separated Values (CSV) file for user analysis. In addition, the tool also generates a CSV file for each sample, where it reports the state of all network nodes after each update cycle.

3.2. Knockout Simulation

The PseudoCell tool additionally enables the assessment of the dynamic consequences following the removal of any given node in the network. This functionality is facilitated through the Node Configurations sub-module, whereby the user can select and knockout any node in the network. This action sets the state of the selected node to a permanent zero, simulating the effect of a gene or protein knockout or metabolite depletion. The ability to perform such simulations offers the means to analyze the impact of node deletion on the overall network dynamics.

3.3. Collaborative Network Creation

A key function of the tool is the expansion and collaborative curation of the network. In this sense, the software allows and encourages the collaboration of community members in order to expand and increase the robustness and reliability of the generated network. To accomplish this goal, the software provides intuitive and flexible graphical interfaces for managing and modifying the nodes and rules of the network, which are central to the scalability of the tool. All changes are recorded in an extensible markup language (XML) file, ensuring that they can be restored in future analyses. Users are encouraged to share their personalized networks with the community through the tool's website (isenesc.com.br/pages/tools.php). By doing so, they can contribute to a collaborative effort that expands and enhances the network, making it possible to evaluate an increasing number of pathways and outcomes. This feature of the PseudoCell network guarantees its capacity to evolve and expand its scope and robustness, providing increased reliability to the network through the correction and improvement process carried out by the user community.

4. Validation of the tool PseudoCell in a model of increasing concentrations of CCL11

Allergic asthma is a complex and heterogeneous inflammatory airway disease where eosinophil-mediated secretion of C-C molecule Motif Chemokine Ligand 11 (CCL11, eotaxin-1) plays a critical role. Initially, CCL11 was proposed as a chemokine associated with eosinophil recruitment through its binding to the C–C chemokine receptor 3 (CCR3) (Park et al., 2017; Sallusto et al., 1997). However, subsequent studies have shown that this chemokine is also associated with multiple biological phenomena, such as endothelial cell migration, and angiogenesis promotion (Kodali et al., 2004; Salcedo et al., 2001).

While several potentially important pathways have been identified, the intracellular implications of the CCR3-CCL11 binding and their relationship with the phenotypic and functional changes observed at the cellular level are not fully understood. Among the molecular effectors of this binding, studies demonstrate a dose-dependent activation of pathways such as PI3K/AKT and MAPK14 (P38). Activation of these pathways is directly associated with cell migration in different cell types and may induce eosinophil degranulation (Badewa & Heiman, 2003a; Kampen et al., 2000a; Mishra et al., 2005).

In a broader spectrum, CCL11 also appears to act on the cellular senescence process as an aging factor. Villeda et al. (2011) demonstrated that, in young mice, the serum increase of this chemokine impairs neurogenesis, learning, and memory associated with aging. This relationship seems to be central in pathological conditions associated with aging, such as severe or treatment-refractory asthma. In these individuals, as opposed to treatment-responsive cases, levels of CCL11 circulating in peripheral blood are negatively correlated with telomere length, an important marker of cellular aging (Barbé-Tuana et al., 2021). Furthermore, evidence corroborates the association of CCL11 with aging and senescence by demonstrating the age-dependent increase of this molecule in human peripheral blood (Hoefer et al., 2017). Despite this, little is known about the molecular and intracellular events that explain the association of this chemokine with cellular aging.

In order to validate the PseudoCell tool's capacity to emulate a biological system, we sought to evaluate molecular aspects associated with increasing concentrations of the CCL11 and compare them with the findings evidenced in the literature. For this purpose, PseudoCell's logical network was stimulated by the activation of the CCL11 node in increasing frequencies. The activation frequencies of nodes in the PI3K/AKT and MAPK14 pathways were then evaluated, and the results were compared with those expected according to the literature (Badewa & Heiman, 2003a; Kampen et al., 2000a;

Mishra et al., 2005). Furthermore, we also sought to demonstrate the predictive capacity of the tool by exploring the molecular mechanisms that may be involved in differential aging between patients with severe and moderate asthma.

4.1. CCL11 promotes dose-dependent activation of the PI3K/AKT and MAPK14 pathways *in silico*

First, we sought to validate the software's potential to simulate results found experimentally in the literature. To this end, the logic network was stimulated with perturbations of the CCL11 node at increasing frequencies: 100% (constitutive expression), 50% (high expression), 25% (medium expression), 12.5% (low expression), and 0% (control). The network was then updated for 1,000 cycles and the simulations were repeated 30 times (n=30) for each experimental group.

In order to compare the results found in the simulations with those expected by the literature, we assessed the activation frequency of nodes associated with the PI3K/AKT and MAPK14 pathways. In this experiment, we verified a dose-dependent increase in PI3K, AKT, ERK1, ERK2, and MAPK14 nodes (Figure 3). These results are in line with the literature, where an increase in the expression or phosphorylation of these proteins was observed after stimulation with CCL11 (Badewa & Heiman, 2003b; Kampen et al., 2000b; Miyagaki et al., 2011; Park et al., 2017).

4.2. CCL11 promotes ROS-mediated DNA damage at high concentrations *in silico*

Furthermore, we assessed the tool's capacity to clarify causality relationships between different cellular outcomes. In this sense, we sought to determine regulatory pathways that would help us understand the molecular mechanisms that underlie the differential aging in patients with severe asthma compared to those with mild asthma (Barbé-Tuana et al., 2021; Isgrò et al., 2013; D. Wu et al., 2014). To achieve this, we employed the previously presented model, where PseudoCell's logical network was stimulated with increasing frequencies of CCL11. The network’s nodes activation frequency was expressed as a heatmap where the rows represent the nodes that had a variation greater than zero and the columns represent the experimental groups (Figure 4A and Supplementary Table 1S). By analyzing the node activation frequencies, we identified clusters where nodes appeared to exhibit a buffering effect in response to CCL11 stimulation. That is, its activation remained at the baseline level at the lower frequencies but increased when challenged with higher frequencies.

To assess which pathways or biological functions could explain this phenomenon, we performed an overrepresentation analysis preceded by a differential activation analysis of the network nodes. Specifically, we considered only those nodes that had their activation altered in the group subjected to the highest, but not in the to the lowest frequencies of CCL11 (Figure 4B and Supplementary Table 2S). These analyses were performed using R language, RStudio integrated development environment, and the clusterProfiler (T. Wu et al., 2021; Yu et al., 2012) and limma packages (Ritchie et al., 2015). Our analysis revealed pathways and biological functions that were significantly enriched in the high-frequency group compared to the low-frequency group (Figure 4C and Supplementary Table 3S).

Among the main pathways, it is possible to verify an important prevalence of those associated with DNA damage and repair (Figure 4C). This finding is expressed by an increased frequency of activation of nodes such as Double Strand Break (DSB), Ataxia Telangiectasia Mutated (ATM), and H2A Histone Family Member X (H2AX) (Figure 4D). Based on that, it is possible to assume that one of the mechanisms involved in the pathological differences between different concentrations of CCL11 is the generation of DNA damage. Furthermore, there was an increase in the activation of nodes associated with the reactive oxygen species (ROS) production pathway, such as the Superoxide node ($O_2^{-\cdot}$) and the genes that codify for NADPH Oxidase 2 (CYBB) and Rac Family Small GTPase 1 (RAC1) (Figure 4D).

4.3. Suppression of ROS production *in silico* inhibits activation of nodes associated with DNA damage

In order to verify the causal relationship between ROS production in CCL11 pathway activation and the promotion of DNA damage, the system was challenged with increasing frequencies of CCL11 node activation associated with superoxide node knockout. The results were expressed in the form of a heatmap (Figure 5A).

In this analysis, CYBB knockout, which encodes for the protein gp-91phox, the beta subunit of the NADPH oxidase enzyme, necessary for the formation of ROS through the activation of the CCL11 pathway, inhibited the activation of nodes associated with the DNA damage response (DSB, ATM, and H2AX) (Figure 5B). Furthermore, despite suppressing CCL11-dependent increase in superoxide node activity, CYBB knockout does not interfere with the activation of pathway upstream elements, such as RAC1

(Figure 5B). This relationship allows us to hypothesize that DNA damage promoted by high concentrations of CCL11 can be explained by the increase in ROS production.

4.4. CCL11 induces ROS production in PBMC from eutrophic individual

To validate the computational findings, peripheral blood (5 mL) was collected by venipuncture into EDTA tubes from a healthy, eutrophic 28-year-old subject with no chronic inflammatory conditions. The protocol was approved by the Internal Review Board from Pontifícia Universidade Católica do Rio Grande do Sul (29576014.4.1001.5336). PBMC were isolated by density gradient (Histopaque 1.077 g/mL; Sigma Aldrich) according to the manufacturer's instructions. Purified PBMC were counted with trypan blue and viable cells (> 95%) were used for subsequent experiments.

PBMC were cultured in 96 well plates ($5x10^4$ cells/well) and treated with increasing concentrations (125 ng/10^5cells/mL, 250 ng/10^5cells/mL, and 500 ng/10^5cells/mL) of recombinant human CCL11 (rhCCL11, Peprotech, Brazil) diluted in HBSS (Sigma Aldrich). Immediately after treatment, cells were incubated with 10 µM 2′-7′-dichlorofluorescein diacetate (DCFH-DA, Sigma Inc.) for ROS quantification. The fluorescence generated by the probe in response to oxidative metabolism was measured using a 96-well microplate reader (VICTOR X Multilabel Plate Readers, PerkinElmer Inc.) at 485/535 nm (excitation/emission). One hundred eighty (180) readings were performed in a 300 minutes interval. The results were expressed as relative fluorescence units (RFU).

Here, eotaxin-1/CCL11 induced the secretion of ROS at medium dose (250 ng/10^5cells/mL) 120 minutes after incubation and at the higher dose (500 ng/10^5cells/mL) after 30 minutes of stimuli ($p < 0.0001$) (Figure 6A). Furthermore, when we analyzed the area under the curve (AUC), we observed higher ROS production with medium and high-CCL11 ($p < 0.0001$) concentrations (Figure 6B, C), pointing out to a dose-dependent mechanism in response to eotaxin-1/CCL11. Interestingly, 180 minutes after treatment, the higher dose of CCL11 (500 ng/10^5cells/mL) was similar to the positive control with 100 µM H_2O_2, suggesting an important role of eotaxin-1/CCL11 in ROS production.

4.5. CCL11 induces activation of H2AX and TP53 via ROS in PBMC

In order to verify if the oxidative stress triggered by CCL11 stimulation induces the activation of pathways associated with cell damage, PBMC were cultured in 24-well-

plate at $0.1x10^6$ cells/mL and treated with rhCCL11 at 500 ng/10^5cells/mL and 5 mM N-Acetyl Cysteine (NAC, Sigma Aldrich) for 2 hours in RPMI-1640 medium (Sigma Aldrich) supplemented with 10% FBS. Cells were washed twice with FACS buffer (saline supplemented with 2% of FBS), fixed with BD Cytofix™ Fixation Buffer (BD Biosciences) for 20 minutes at 4°C and permeabilized with BD Phosflow™ Perm Buffer III (BD Biosciences) for 30 minutes at 4°C. Cells were then washed again with FACS Buffer and incubated with an antibody mix containing Alexa Fluor® 647 Mouse anti-H2AX (pS139) 1:200 (#560447 BD Biosciences) and Alexa Fluor® 488 Mouse anti-p53 (pS37) 1:50 (#560282 BD Biosciences) for 30 minutes at 4°C. Finally, cells were washed and resuspended in FACS buffer for acquisition (10,000 events). Acquisitions were made in a BD FACSCanto™ II (BD Biosciences) with a 3-laser, 4-2-2 configuration (Violet 405 nm, Blue 488 nm, and Red 633 nm). FACS data was analyzed with FlowJo™ v10.8.1 (BD Life Sciences).

We observed an increase in the activity (phosphorylation) of γH2AX after treatment with CCL11 500 ng/mL, which was prevented by the co-treatment with the antioxidant molecule NAC ($p = 0.0012$) (Figure 6D). In addition, we observed increased TP53 phosphorylation after treatment with CCL11 ($p = 0.0004$) (Figure 6E). These results suggest an important role of eotaxin-1/CCL11 in DNA damage signaling pathways activation, which is partially prevented by ROS depletion with NAC. Our results strongly correlate with those seen in the *in silico* CYBB knockout model, denoting PseudoCell as a useful tool with significant predictive capability.

5. Conclusion

In conclusion, the PseudoCell tool uses validated biological knowledge to simulate complex biological systems and predict their behavior under various conditions. The validation of PseudoCell's logical network through comparison with experimental data from the literature confirms its ability to emulate key molecular aspects of the system under study. Moreover, we tested the predictive capacity of PseudoCell through its ability to generate valid hypotheses about the molecular mechanisms. In this regard, we suggest a new and underlying molecular signaling pathway of premature aging in patients with severe and moderate asthma through CCL11 stimulation. We believe that PseudoCell can be a valuable resource for researchers in the fields of systems biology and can help to advance our understanding of the complexity of biological systems. Future research could

further validate and refine the PseudoCell tool, as well as apply it to other biological conditions of interest.

AVAILABILITY

PseudoCell is a free open-source regulatory network and simulation tool available in PseudoCell website (http://isenesc.com.br/pages/tools.php) or in the GitHub repository (https://github.com/viniciuspierdona/pseudocell).

ACKNOWLEDGEMENT

This research was supported by Pontifícia Universidade Católica do Rio Grande do Sul (PUCRS) and Universidade Federal do Rio Grande do Sul (UFRGS).

FUNDING

This article was supported by grants from Conselho Nacional de Desenvolvimento Científico e Tecnológico (CNPq) and Coordenação de Aperfeiçoamento de Pessoal de Nível Superior-Brasil (CAPES). VP, RMM, and PL received a scholarship from CAPES and CNPq, respectively. JCMM, FTCRG and FMBT are senior investigators from CNPq.

CONFLICT OF INTEREST

None declared.

REFERENCES

Badewa, A. P., & Heiman, A. S. (2003a). Inhibition of CCL11, CCL24, and CCL26-induced degranulation in HL-60 eosinophilic cells by specific inhibitors of MEK1/MEK2, p38 MAP kinase, and PI 3-kinase. *Immunopharmacology and Immunotoxicology*, *25*(2), 145–157. https://doi.org/10.1081/IPH-120020466

Badewa, A. P., & Heiman, A. S. (2003b). Inhibition of CCL11, CCL24, and CCL26-induced degranulation in HL-60 eosinophilic cells by specific inhibitors of MEK1/MEK2, p38 MAP kinase, and PI 3-kinase. *Immunopharmacology and Immunotoxicology*, *25*(2), 145–157. https://doi.org/10.1081/IPH-120020466

Barabási, A. L., & Oltvai, Z. N. (2004). Network biology: understanding the cell's functional organization. *Nature Reviews Genetics 2004 5:2*, *5*(2), 101–113. https://doi.org/10.1038/nrg1272

Barbé-Tuana, F. M., Grun, L. K., Pierdoná, V., Parisi, M. M., Friedrich, F., Guma, F. T. C. R., Pinto, L. A., Stein, R. T., Pitrez, P. M. C., & Jones, M. H. (2021). Shorter telomeres in children with severe asthma, an indicative of accelerated aging. *Aging (Albany NY)*, *13*(2), 1686. https://doi.org/10.18632/AGING.202527

Béal, J., Pantolini, L., Noël, V., Barillot, E., & Calzone, L. (2021). Personalized logical models to investigate cancer response to BRAF treatments in melanomas and colorectal cancers. *PLOS Computational Biology*, *17*(1), e1007900. https://doi.org/10.1371/JOURNAL.PCBI.1007900

Bhalla, U. S., & Iyengar, R. (1999). Emergent properties of networks of biological signaling pathways. *Science (New York, N.Y.)*, *283*(5400), 381–387. https://doi.org/10.1126/SCIENCE.283.5400.381

Bizzarri, M., Palombo, A., & Cucina, A. (2013). Theoretical aspects of Systems Biology. *Progress in Biophysics and Molecular Biology*, *112*(1–2), 33–43. https://doi.org/10.1016/j.pbiomolbio.2013.03.019

Coveney, P. v., & Fowler, P. W. (2005). Modelling biological complexity: a physical scientist's perspective. *Journal of The Royal Society Interface*, *2*(4), 267–280. https://doi.org/10.1098/RSIF.2005.0045

Elowitz, M. B. (2013). *Stochastic Gene Expression in a Single Cell*. *1183*(2002). https://doi.org/10.1126/science.1070919

Fisher, J., & Henzinger, T. A. (2007). Executable cell biology. *Nature Biotechnology 2007 25:11*, *25*(11), 1239–1249. https://doi.org/10.1038/nbt1356

Fisher, J., Piterman, N., & Bodik, R. (2014). Toward synthesizing executable models in biology. *Frontiers in Bioengineering and Biotechnology*, *2*(DEC), 75. https://doi.org/10.3389/FBIOE.2014.00075/BIBTEX

Gupta, S., & Hashimoto, R. F. (2022). Dynamical Analysis of a Boolean Network Model of the Oncogene Role of lncRNA ANRIL and lncRNA UFC1 in Non-Small Cell Lung Cancer. *Biomolecules*, *12*(3), 420. https://doi.org/10.3390/BIOM12030420/S1

Gupta, S., Panda, P. K., Luo, W., Hashimoto, R. F., & Ahuja, R. (2022). Network analysis reveals that the tumor suppressor lncRNA GAS5 acts as a double-edged sword in response to DNA damage in gastric cancer. *Scientific Reports 2022 12:1*, *12*(1), 1–10. https://doi.org/10.1038/s41598-022-21492-x

Gupta, S., Silveira, D. A., & Mombach, J. C. M. (2020a). ATM/miR-34a-5p axis regulates a p21-dependent senescence-apoptosis switch in non-small cell lung cancer: a Boolean model of G1/S checkpoint regulation. *FEBS Letters*, *594*(2), 227–239. https://doi.org/10.1002/1873-3468.13615

Gupta, S., Silveira, D. A., & Mombach, J. C. M. (2020b). Towards DNA-damage induced autophagy: A Boolean model of p53-induced cell fate mechanisms. *DNA Repair*, *96*, 102971. https://doi.org/10.1016/J.DNAREP.2020.102971

Helikar, T., Kowal, B., McClenathan, S., Bruckner, M., Rowley, T., Madrahimov, A., Wicks, B., Shrestha, M., Limbu, K., & Rogers, J. A. (2012). The Cell Collective: Toward an open and collaborative approach to systems biology. *BMC Systems Biology*, *6*(1), 1–14. https://doi.org/10.1186/1752-0509-6-96/FIGURES/8

Hoefer, J., Luger, M., Dal-Pont, C., Culig, Z., Schennach, H., & Jochberger, S. (2017). The "aging factor" eotaxin-1 (CCL11) is detectable in transfusion blood products and increases with the donor's age. *Frontiers in Aging Neuroscience*, *9*(DEC). https://doi.org/10.3389/FNAGI.2017.00402/FULL

Isgrò, M., Bianchetti, L., Marini, M. A., Bellini, A., Schmidt, M., & Mattoli, S. (2013). The C-C motif chemokine ligands CCL5, CCL11, and CCL24 induce the migration of circulating fibrocytes from patients with severe asthma. *Mucosal Immunology*, *6*(4), 718–727. https://doi.org/10.1038/MI.2012.109/ATTACHMENT/5B050700-7CD9-4F87-B8E3-495CEF148E6E/MMC9.PPT

Jordan, J. D., Landau, E. M., & Iyengar, R. (2000). Signaling Networks: The Origins of Cellular Multitasking. *Cell*, *103*(2), 193–200. https://doi.org/10.1016/S0092-8674(00)00112-4

Kampen, G. T., Stafford, S., Adachi, T., Jinquan, T., Quan, S., Grant, J. A., Skov, P. S., Poulsen, L. K., & Alam, R. (2000a). Eotaxin induces degranulation and chemotaxis of eosinophils through the activation of ERK2 and p38 mitogen-activated protein kinases. *Blood*, *95*(6), 1911–1917. https://doi.org/10.1182/BLOOD.V95.6.1911

Kampen, G. T., Stafford, S., Adachi, T., Jinquan, T., Quan, S., Grant, J. A., Skov, P. S., Poulsen, L. K., & Alam, R. (2000b). Eotaxin induces degranulation and chemotaxis of eosinophils through the activation of ERK2 and p38 mitogen-activated protein kinases. *Blood*, *95*(6), 1911–1917. https://doi.org/10.1182/blood.v95.6.1911

Kitano, H. (2002a). Systems Biology: A Brief Overview. *Science*, *295*(5560), 1662–1664. https://doi.org/10.1126/SCIENCE.1069492

Kitano, H. (2002b). Computational systems biology. In *Nature* (Vol. 420, Issue 6912, pp. 206–210). https://doi.org/10.1038/nature01254

Kodali, R. B., Kim, W. J. H., Galaria, I. I., Miller, C., Schecter, A. D., Lira, S. A., & Taubman, M. B. (2004). CCL11 (Eotaxin) induces CCR3-dependent smooth muscle cell migration. *Arteriosclerosis, Thrombosis, and Vascular Biology*, *24*(7), 1211–1216. https://doi.org/10.1161/01.ATV.0000131654.90788.F5

Mazzocchi, F. (2008). Complexity in biology. Exceeding the limits of reductionism and determinism using complexity theory. *EMBO Reports*, *9*(1), 10. https://doi.org/10.1038/SJ.EMBOR.7401147

Mishra, R. K., Scaife, J. E., Harb, Z., Gray, B. C., Djukanovic, R., & Dent, G. (2005). Differential dependence of eosinophil chemotactic responses on phosphoinositide 3-kinase (PI3K). *Allergy*, *60*(9), 1204–1207. https://doi.org/10.1111/J.1398-9995.2005.00845.X

Miyagaki, T., Sugaya, M., Murakami, T., Asano, Y., Tada, Y., Kadono, T., Okochi, H., Tamaki, K., & Sato, S. (2011). CCL11-CCR3 interactions promote survival of anaplastic large cell lymphoma cells via ERK1/2 activation. *Cancer Research*, *71*(6), 2056–2065. https://doi.org/10.1158/0008-5472.CAN-10-3764

Naldi, A., Hernandez, C., Abou-Jaoudé, W., Monteiro, P. T., Chaouiya, C., & Thieffry, D. (2018). Logical modeling and analysis of cellular regulatory networks with GINsim 3.0. *Frontiers in Physiology*, *9*(JUN), 646. https://doi.org/10.3389/FPHYS.2018.00646/BIBTEX

Ostaszewski, M., Niarakis, A., Mazein, A., Kuperstein, I., Phair, R., Orta-Resendiz, A., Singh, V., Aghamiri, S. S., Acencio, M. L., Glaab, E., Ruepp, A., Fobo, G., Montrone, C., Brauner, B., Frishman, G., Gómez, L. C. M., Somers, J., Hoch, M., Gupta, S. K., … Schneider, R. (2021). COVID19 Disease Map, a computational knowledge repository of virus–host interaction mechanisms. *Molecular Systems Biology*, *17*(10), e10387. https://doi.org/10.15252/MSB.202110387

Park, J. Y., Kang, Y. W., Choi, B. Y., Yang, Y. C., Cho, B. P., & Cho, W. G. (2017). CCL11 promotes angiogenic activity by activating the PI3K/Akt pathway in HUVECs. *Journal of Receptor and Signal Transduction Research*, *37*(4), 416–421. https://doi.org/10.1080/10799893.2017.1298132

Ritchie, M. E., Phipson, B., Wu, D., Hu, Y., Law, C. W., Shi, W., & Smyth, G. K. (2015). limma powers differential expression analyses for RNA-sequencing and microarray studies. *Nucleic Acids Research*, *43*(7), e47–e47. https://doi.org/10.1093/NAR/GKV007

Rodríguez-Jorge, O., Kempis-Calanis, L. A., Abou-Jaoudé, W., Gutiérrez-Reyna, D. Y., Hernandez, C., Ramirez-Pliego, O., Thomas-Chollier, M., Spicuglia, S., Santana, M. A., & Thieffry, D. (2019). Cooperation between T cell receptor and Toll-like receptor 5 signaling for CD4+ T cell activation. *Science Signaling*, *12*(577). https://doi.org/10.1126/SCISIGNAL.AAR3641/SUPPL_FILE/AAR3641_SM.PDF

Saadatpour, A., & Albert, R. (2013). Boolean modeling of biological regulatory networks: A methodology tutorial. *Methods*, *62*(1), 3–12. https://doi.org/10.1016/J.YMETH.2012.10.012

Salcedo, R., Young, H. A., Ponce, M. L., Ward, J. M., Kleinman, H. K., Murphy, W. J., & Oppenheim, J. J. (2001). Eotaxin (CCL11) induces in vivo angiogenic responses by human CCR3+ endothelial cells. *Journal of Immunology (Baltimore, Md. : 1950)*, *166*(12), 7571–7578. https://doi.org/10.4049/JIMMUNOL.166.12.7571

Sallusto, F., Mackay, C. R., & Lanzavecchia, A. (1997). Selective expression of the eotaxin receptor CCR3 by human T helper 2 cells. *Science (New York, N.Y.)*, *277*(5334), 2005–2007. https://doi.org/10.1126/SCIENCE.277.5334.2005

Samaga, R., & Klamt, S. (2013). Modeling approaches for qualitative and semi-quantitative analysis of cellular signaling networks. In *Cell Communication and Signaling* (Vol. 11, Issue 1). https://doi.org/10.1186/1478-811X-11-43

Silveira, D. A., Gupta, S., & Mombach, J. C. M. (2020). Systems biology approach suggests new miRNAs as phenotypic stability factors in the epithelial–mesenchymal transition. *Journal of the Royal Society Interface*, *17*(171). https://doi.org/10.1098/RSIF.2020.0693

Villeda, S. A., Luo, J., Mosher, K. I., Zou, B., Britschgi, M., Bieri, G., Stan, T. M., Fainberg, N., Ding, Z., Eggel, A., Lucin, K. M., Czirr, E., Park, J. S., Couillard-Després, S., Aigner, L., Li, G., Peskind, E. R., Kaye, J. A., Quinn, J. F., … Wyss-Coray, T. (2011). The aging systemic milieu negatively regulates neurogenesis and cognitive function. *Nature*, *477*(7362), 90. https://doi.org/10.1038/NATURE10357

Wu, D., Zhou, J., Bi, H., Li, L., Gao, W., Huang, M., Adcock, I. M., Barnes, P. J., & Yao, X. (2014). CCL11 as a potential diagnostic marker for asthma? *Http://Dx.Doi.Org/10.3109/02770903.2014.917659*, *51*(8), 847–854. https://doi.org/10.3109/02770903.2014.917659

Wu, T., Hu, E., Xu, S., Chen, M., Guo, P., Dai, Z., Feng, T., Zhou, L., Tang, W., Zhan, L., Fu, X., Liu, S., Bo, X., & Yu, G. (2021). clusterProfiler 4.0: A universal enrichment tool for interpreting omics data. *The Innovation*, *2*(3), 100141. https://doi.org/10.1016/j.xinn.2021.100141

Yu, G., Wang, L. G., Han, Y., & He, Q. Y. (2012). ClusterProfiler: An R package for comparing biological themes among gene clusters. *OMICS A Journal of Integrative Biology*, *16*(5), 284–287. https://doi.org/10.1089/OMI.2011.0118/ASSET/IMAGES/LARGE/FIGURE1.JPEG

TABLE AND FIGURES LEGENDS

Figure 1. Topological structure of the constructed network. The interaction graph is built from the logical model, where proteins, genes, metabolites, and other biological elements are represented by circular nodes. Green edges represent the positive connections, while the red ones represent the negative connections.

Figure 2. PseudoCell tool architecture. The tool is organized into three modules, User Interface, Core Simulator, and Importing/Exporting Module. The User Interface module is responsible for handling the user's experimental conditions. The Core Simulator module is responsible for carrying out the network update iterations based on the logic rules described. The Import/Export Module handles the functions for sharing the networks created by the community. The tool returns a matrix of activation frequency values as output, where the lines represent the samples (S1, S2….Sn) and the columns (n1, n2…nn) the network nodes.

Figure 3. CCL11 induces activation of nodes associated with PI3K/AKT and MAPK14 pathways in PseudoCell's network. The PI3K, AKT1, ERK1, ERK2, and MAPK14 nodes had their activity modulated in a frequency-dependent manner when disturbed by CCL11. Data presented as mean ± Standard Deviation.

Figure 4. Computational evaluation of increasing frequency of CCL11 node activation. **A.** Heatmap representing alteration in activation frequency patterns for Control, CCL11 Low, CCL11 Medium, CCL11 High, and CCL11 Constitutive groups. **B.** Vulcano plot showing the differentially activated nodes in CCL11 Low, CCL11 Medium, CCL11 High, and CCL11 Constitutive in contrast to Control (p-Value<0.01 and |FC|>0.05). Negative FC values were considered downregulated, while positive values were considered upregulated. **C**. Top enriched pathways from the list of genes present at the intersection between the nodes that had their activity altered in CCL11 High and those that did not have their activity altered in the lower frequency groups. **D.** Higher CCL11 activation frequencies (100%, 50%, and 25%) induce an increase in DSB, ATM, and H2AX nodes

activation ($p<0.0001$), while lower frequencies are not able to induce its activation. Differences were analyzed with Kruskal-Wallis test and Dunn's post-hoc comparisons. Data presented as mean ± Standard Deviation.

Figure 5. Effects of CYBB node suppression on ROS production and activation of nodes associated with DNA damage. **A.** Heatmap representing alteration in activation frequencies patterns for Control, CCL11 Low, CCL11 Medium, CCL11 High, and CCL11 Constitutive groups upon CYBB knockout. **B.** CYBB knockout suppresses activation of nodes associated with DNA damage, DSB, ATM and H2AX. CYBB knockout suppresses activation of the superoxide node, but not RAC1. Differences were analyzed with Kruskal-Wallis test and Dunn's post-hoc comparisons. Data presented as mean ± Standard Deviation.

Figure 6. Increasing concentrations of recombinant CCL11 induces ROS formation and DNA damage in PBMC. PBMC were cultured ($5x10^4$ cells/well) in 96 well plate and treated with increasing concentrations of rhCCL11 (low: 125 ng/10^5cells/mL, medium: 250 ng/10^5cells/mL, and high: 500 ng/10^5cells/mL) **A.** Time course of ROS production quantified via DCF-DA assay after stimulation with increasing concentrations of CCL11. Cells were analyzed using total fluorescence assay in the 96-well plate format at 485/535 nm for 300 minutes. **B.** Absolute ROS quantification from area under the curve (AUC) analysis. **C.** Relative fluorescence (Endpoint, 300 min) of ROS production from DCF-DA assay. **D.** Phosflow analysis showed a significant increase in H2AX phosphorylation (pS139) after stimulation with CCL11 (500 ng/10^5cells/mL) suppressed by co-treatment with NAC (p-value < 0.01). **E.** Phosflow analysis showed a significant increase in TP53 phosphorylation (pS37) after stimulation with CCL11 recombinant (500 ng/10^5cells/mL) (p-value < 0.01). MFI: median fluorescence intensity. Data presented as mean ± Standard Deviation.

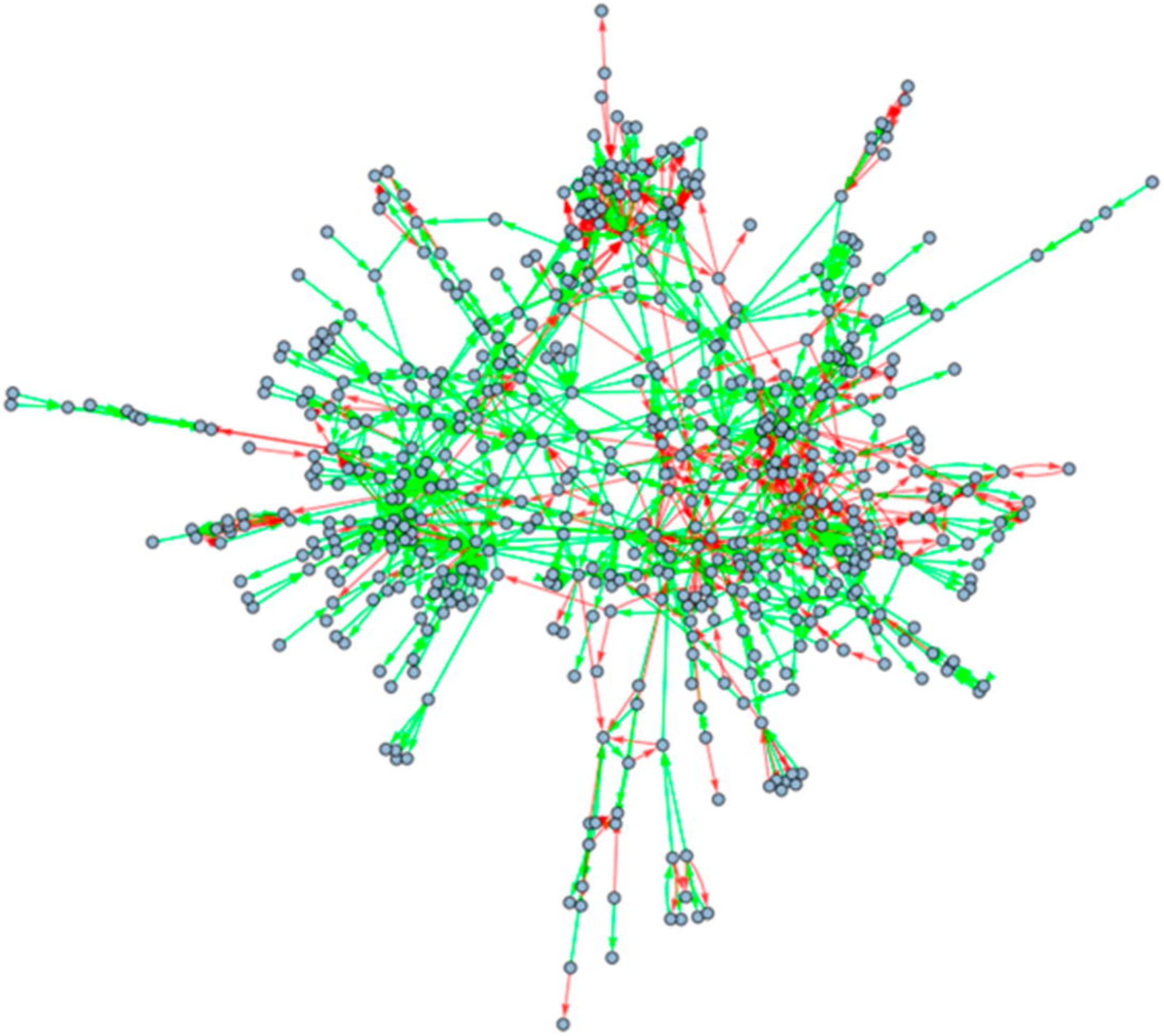

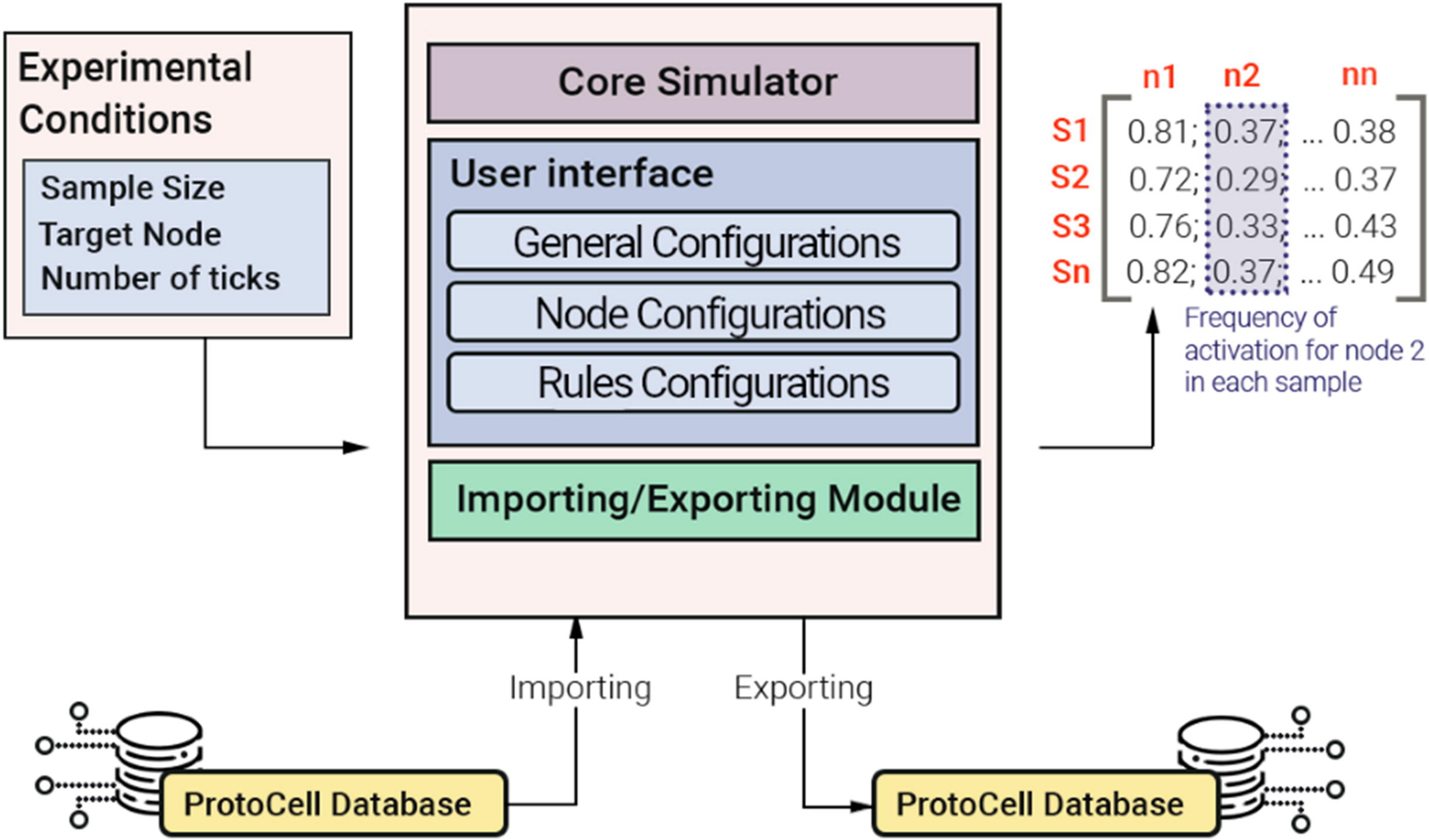
Experimental Conditions
Sample Size
Target Node
Number of ticks
Core Simulator
User interface
General Configurations
Node Configurations
Rules Configurations
Importing/Exporting Module
n1
n2
nn
S1
S2
S3
Sn
0.81; 0.37; ... 0.38
0.72; 0.29; ... 0.37
0.76; 0.33; ... 0.43
0.82; 0.37; ... 0.49
Frequency of activation for node 2 in each sample
Importing
Exporting
ProtoCell Database
ProtoCell Database

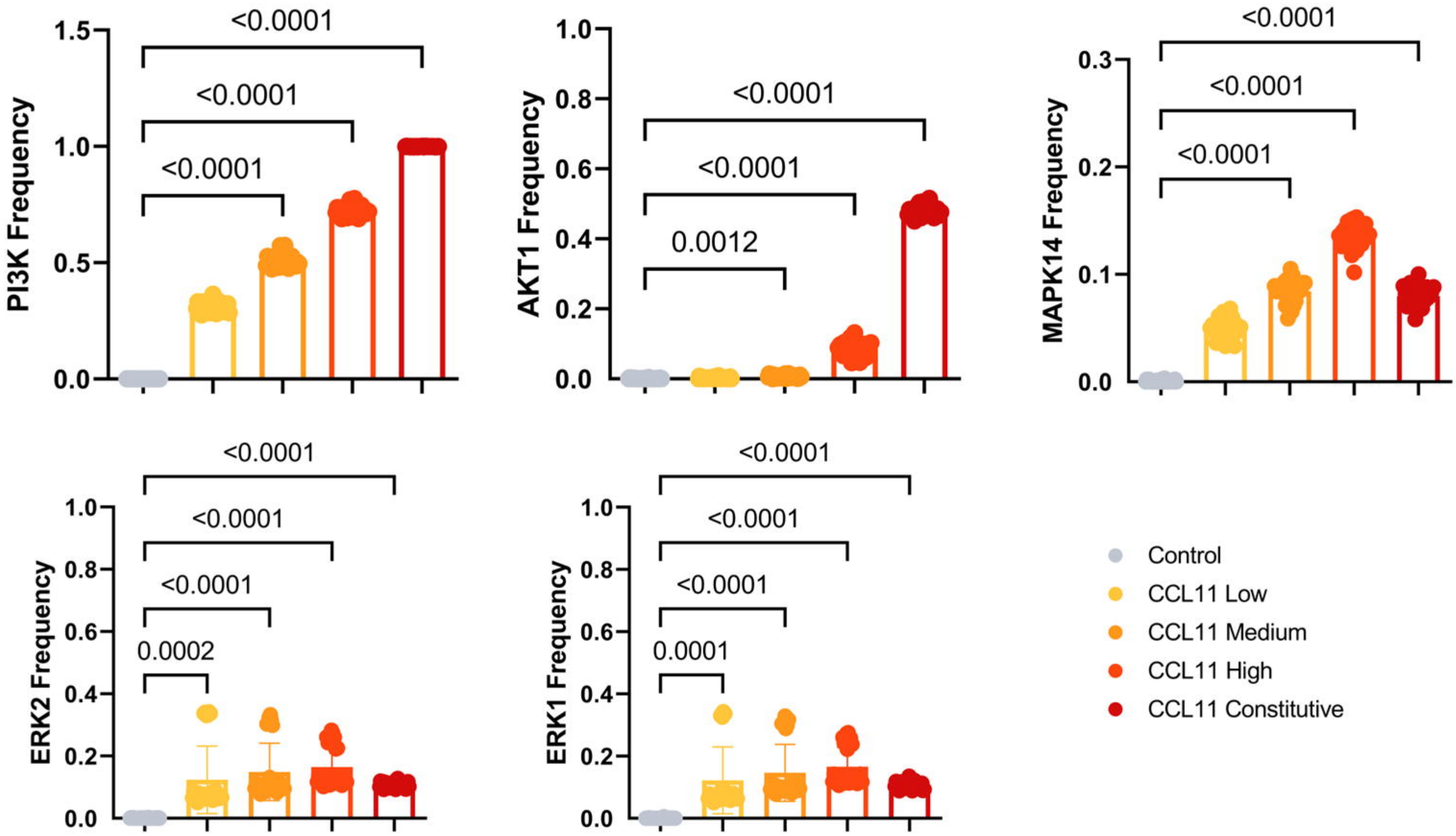
PI3K Frequency
1.5
1.0
0.5
0.0
<0.0001
<0.0001
<0.0001
AKT1 Frequency
1.0
0.8
0.6
0.4
0.2
0.0
<0.0001
<0.0001
0.0012
MAPK14 Frequency
0.3
0.2
0.1
0.0
<0.0001
<0.0001
<0.0001
ERK2 Frequency
1.0
0.8
0.6
0.4
0.2
0.0
<0.0001
<0.0001
<0.0001
0.0002
ERK1 Frequency
1.0
0.8
0.6
0.4
0.2
0.0
<0.0001
<0.0001
<0.0001
0.0001
Control
CCL11 Low
CCL11 Medium
CCL11 High
CCL11 Constitutive

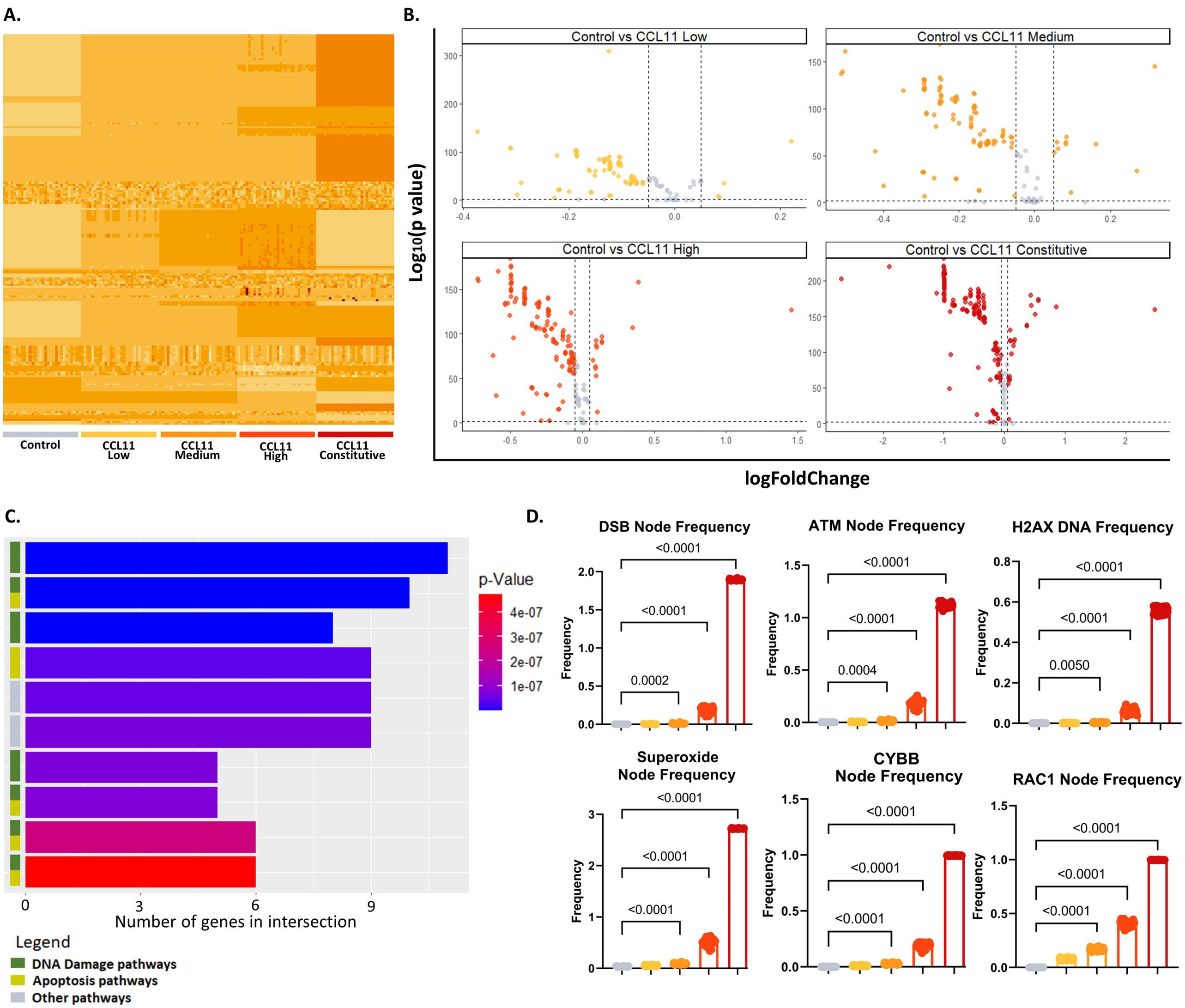
A.
Control
CCL11 Low
CCL11 Medium
CCL11 High
CCL11 Constitutive
B.
Control vs CCL11 Low
Control vs CCL11 Medium
Control vs CCL11 High
Control vs CCL11 Constitutive
Log10(p value)
logFoldChange
C.
p-Value
4e-07
3e-07
2e-07
1e-07
Number of genes in intersection
Legend
DNA Damage pathways
Apoptosis pathways
Other pathways
D.
DSB Node Frequency
ATM Node Frequency
H2AX DNA Frequency
Superoxide Node Frequency
CYBB Node Frequency
RAC1 Node Frequency
Frequency
<0.0001
0.0002
0.0004
0.0050

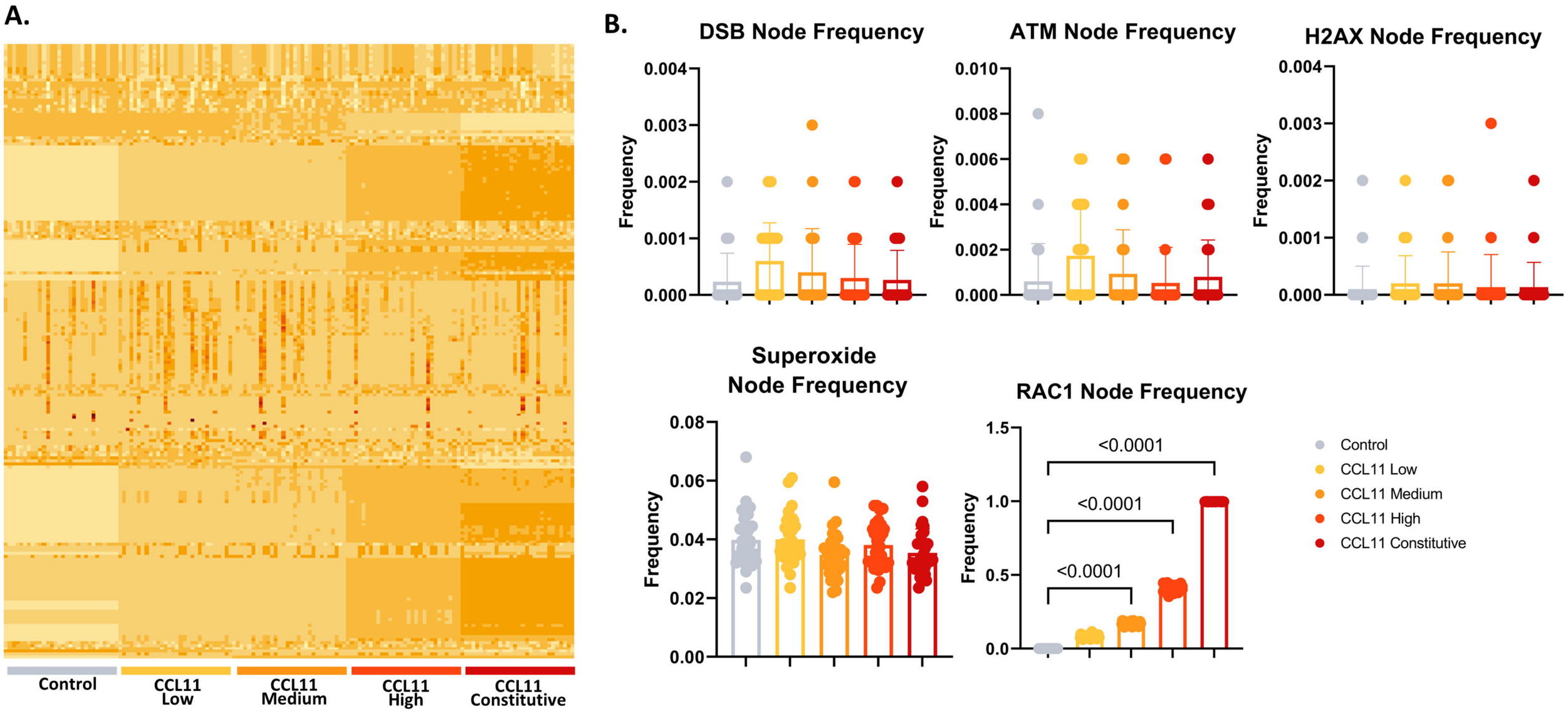
A.
Control
CCL11 Low
CCL11 Medium
CCL11 High
CCL11 Constitutive
B.
DSB Node Frequency
ATM Node Frequency
H2AX Node Frequency
Superoxide Node Frequency
RAC1 Node Frequency
Frequency
<0.0001
<0.0001
<0.0001
Control
CCL11 Low
CCL11 Medium
CCL11 High
CCL11 Constitutive

A.

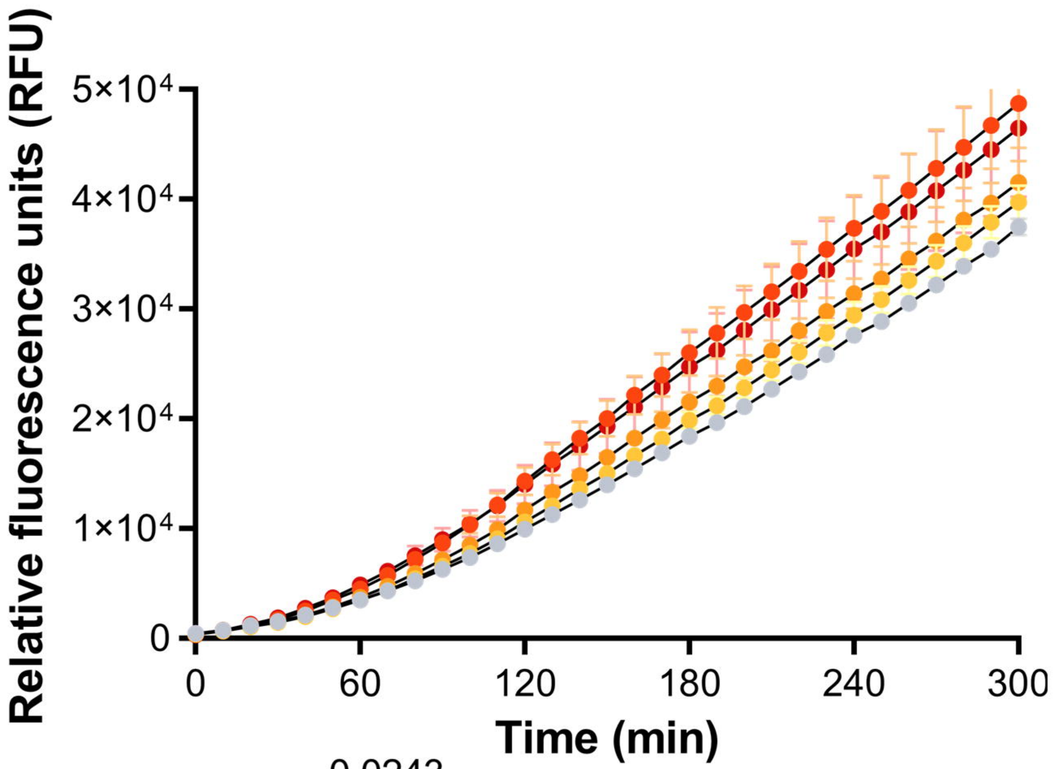
Relative fluorescence units (RFU)
5×10⁴
4×10⁴
3×10⁴
2×10⁴
1×10⁴
0
0
60
120
180
240
300
Time (min)

B.

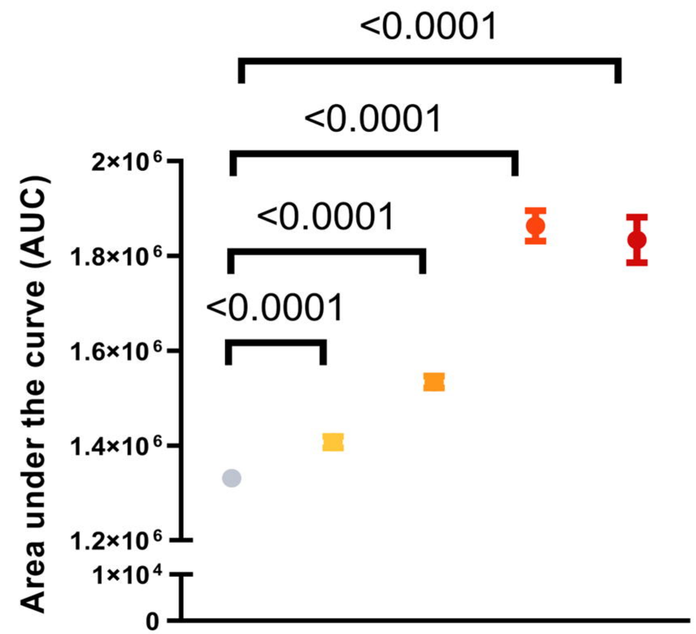
Area under the curve (AUC)
2×10⁶
1.8×10⁶
1.6×10⁶
1.4×10⁶
1.2×10⁶
1×10⁴
0
<0.0001
<0.0001
<0.0001
<0.0001

C.

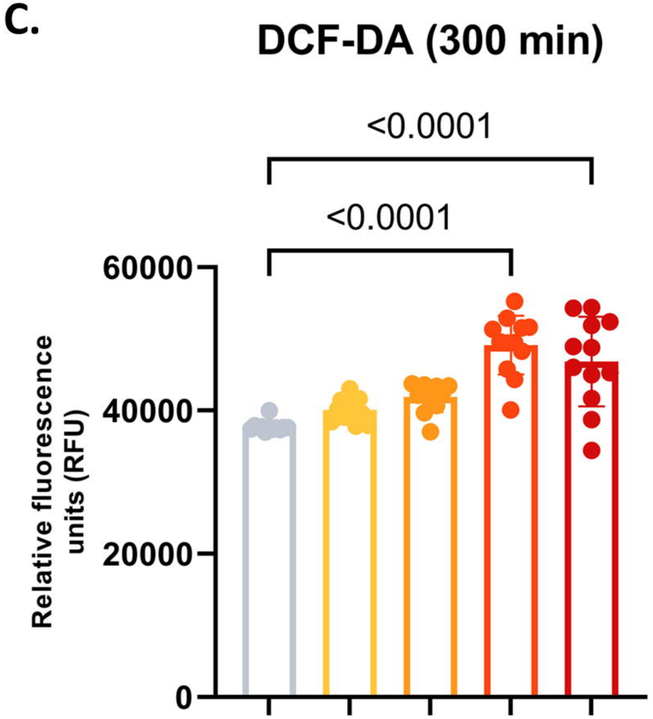
DCF-DA (300 min)
Relative fluorescence units (RFU)
60000
40000
20000
0
<0.0001
<0.0001

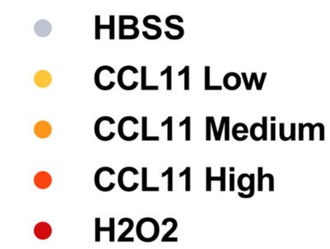
HBSS
CCL11 Low
CCL11 Medium
CCL11 High
H2O2

D.

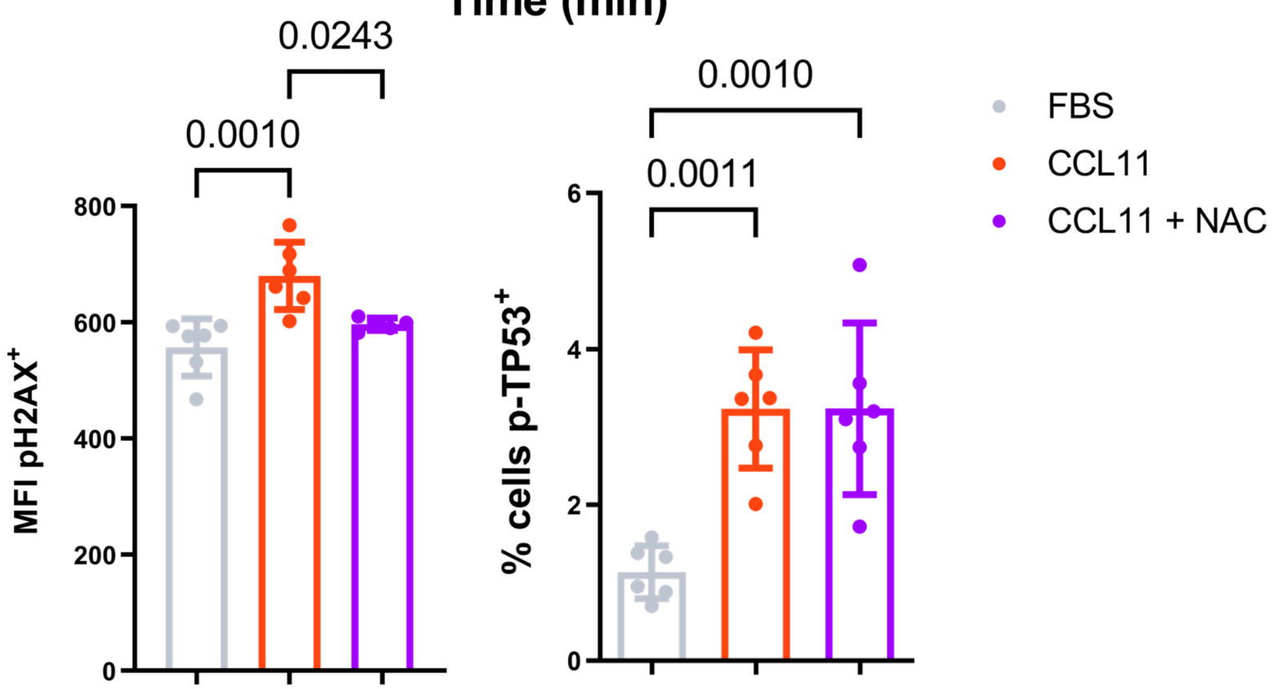
MFI pH2AX⁺
800
600
400
200
0
0.0010
0.0243
% cells p-TP53⁺
6
4
2
0
0.0011
0.0010
FBS
CCL11
CCL11 + NAC